Nanopositioning Control on a Commercial Linear Stage by Software Error Correction

Kuang-Chao Fan[1, 2,a] Fung Chen [1,b], Ye-jin Chen[1,c]

[1] School of Instrumentation, Hefei University of Technology, Anhui, 230009, China
[2] Department of Mechanical Engineering, National Taiwan University, Taipei, Taiwan
Phone: (086)0551-2903817-805 Fax: (086)0551-2903823
E-mail: [a]fan@ntu.edu.tw, [b]chf19chf19@163.com, [c]chenyejin2004@hotmail.com

Abstract:

A digital control scheme of nanopositioning is proposed on a commercially available piezo ceramic linear motor (PCLM) stage equipped with a linear grating of 20μm pitch. Conventional signal subdivision is mostly based on the hardware circuit, which lacks of flexible adjustment when the disturbances are in nanometer scale. This study has developed a LabVIEW-based digital control system, which features the following functions: adjustment of the distorted waveforms, pulse count to the quarter pitch, waveform subdivision by Lissajous circle, back propagation neural network and PID control, and the position feedback control of the stage. Three steps of positioning control are proposed, namely, the AC mode in continuous motion control for the long stroke, the gate mode to drive the motor in low velocities the short stroke, and the DC mode in which the motor works as a piezo actuator, enabling accurate positioning of a few nanometers. In each mode of motion, a particular signal process technique is employed. Experimental results showed this method can easily apply to the studied linear stage to achieve the positioning accuracy within 31nm and standard deviation within 30nm for travels up to 9mm. In comparison with the stage's original specifications of ±1μm repeatability and ±1μm/25mm accuracy this digital control system can upgrade the precision to one order.

Keywords: Nanopositioning, Digital control, Waveform correction, Subdivision, Back propagation neural network, PID control.

Correspondent: Professor Kuang-Chao Fan
                fan@ntu.edu.tw

1. INTRODUCTION

With the rapid development of nanotechnology in IC, micro systems, and Bioscience processes, nanopositioning has become a key technology and challenging task in providing ultraprecision stepping control to the accuracy higher than 100nm and the resolution to 1 nm [1]. Nanopositioning requires a precision motion actuator and a precision position feedback sensor assisted with subdivision technique. Unfortunately, the term nanopositioning is often misused. It is not uncommon to find micropositioning stages, which by definition operate on the micrometer scale, re-labelled as nanopositioning stages in an attempt to make them sound more impressive [2]. At present, the piezo ceramic actuator (PZT) is widely used for fine positioning, but only to the limited stroke length around hundreds of micrometer. Servo motor or stepping motor with ball screw transmission could not generate incremental step in nanometer scale. A stacked up two-stage table comprising of a servo motor stage and a PZT stage is a common solution for long stroke requirement while possessing nanometer step. The mechanical and control systems are, however, too complicated. Using the ultrasonic motor with friction drive mechanism is a possible way to achieve the goal of single stage nanopisitioning. One commercially available linear stage, named by Piezo Ceramic Linear Motor (PCLM) manufactured by the Anorad Co., equipped with an ultrasonic motor made by Nanomotion Co. [7], is able to generate long stroke in centimeter range and fine steps in nanometer range. This stage, however, employs a Renishaw linear scale in 20μm pitch that restricts the resolution to only 0.1μm and the positioning accuracy to ±1μm/25mm with ±1μm repeatability [3]. In order to obtain finer resolution, the subdivision technique has to be employed. The waveform of liner scale may vary due to the motion errors of the stage. Attempting to fit all errors in two simultaneous equations and compensated with waveform correction yields to long computational time [4]. Hardware interpolation is often adopted for fast response [5, 6]. It is, however, sensitive to the dynamic waveforms so as to restrict the positioning accuracy of the stage. The study adopted software waveform process with LabVIEW tool. The distorted waveforms could be corrected by a simple way before the pulse counting and subdivision processes. Thus, the dynamic errors could be removed. In the aspect of motion control, we proposed the three-mode control scheme, namely, the AC mode in continuous

motion fed back by pulse count during the long stroke motion, the gate mode in low velocity fed back by Lissajous diagram based signal interpolation at short stroke motion, and the DC mode for accurate positioning fed back by voltage based curve fitting for nano stroke motion [7]. Besides, in order to get stable signals and to make sure the sampling rate is enough, a low velocity during AC mode is necessary. Classic PID control scheme need three constant parameter K_p , K_i and K_d which should be determined by experiments. A new PID control with BP neural network shows more convenience and robustness [10]. Experimental results showed that this digital control scheme is superior to its original PWM control provided by the company.

2. The Linear Stage and its Driver

Most positioning technologies have to compromise between the stroke length and the positioning precision (accuracy + uncertainty). For the long stroke motion, usually driven by the servomotor and detected by a linear scale, the positioning precision is limited to only micrometer order. For the fine motion, usually driven by the PZT actuator and detected by the capacitance sensor, the stroke is limited to only several hundreds of micrometer. This study aims to a long stroke while possessing fine motion stage, called the Piezo Ceramic Linear Motor (PCLM) made by Anorad Co. Fig. 1 shows the configuration of the PCLM stage. Fig. 2 presents its cross-sectional view, in which a tape scale (made by the Renishaw Co.) with 20μm pitch is mounted underneath the table center. The actuator system consists of an ultrasonic motor and a drive amplifier (model AB1) to excite the motor, supplied by the Nanomotion Co. of Israel. These two components are combined to create the piezoelectric effect. This effect converts electrical field to a mechanical motion. The important role of operation is the 4-piezo elements PCLM (Type HR-4) motor. When the voltage is applying across the element in a precise sequence, the edge of the piezo element generates an elliptical motion, which is the vector sum of the bending mode and the longitudinal mode, as shown in Fig. 3. This elliptical motion then drives the stage by friction force to create linear motion. According to the technical specifications given by the company the stage has resolution of 0.1μm and the positioning accuracy of ±1μm/25mm with ±1μm repeatability when driven by the AC mode. An accuracy test was carried out using the HP 5529 laser interferometer, and the results were confirmed after error compensation, as shown in Fig. 4.
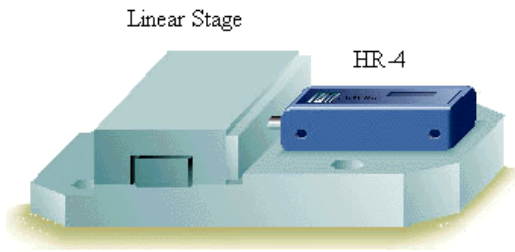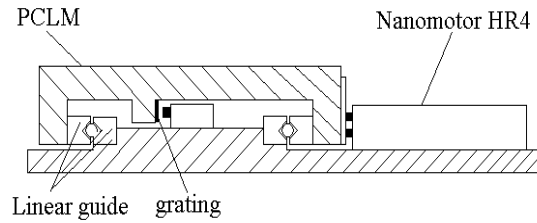
Fig. 1: Structure of the PCLM
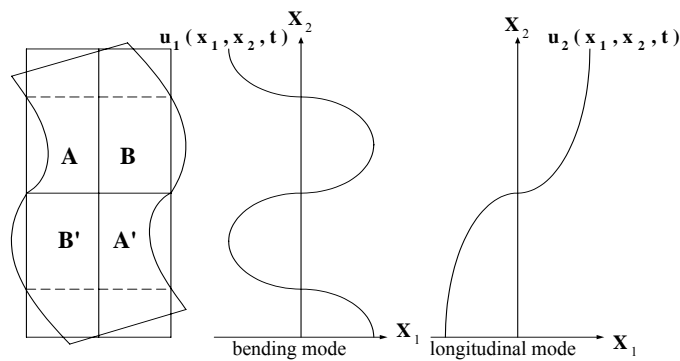

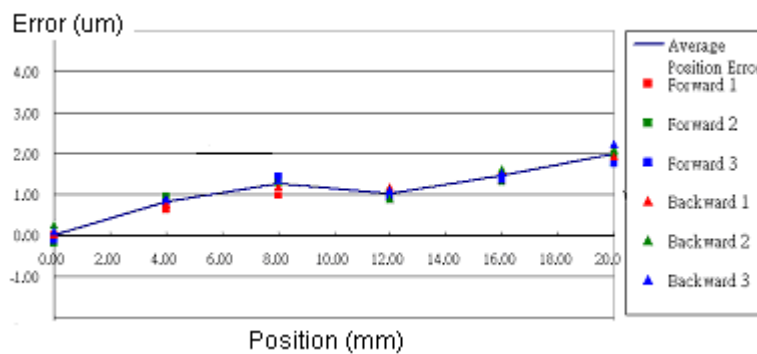Fig. 2: The cross section view of the stage

Fig. 3: AC mode of PCLM

Fig. 4: X-positioning accuracy of PCLM.

The Nanomotion Co. released a new drive after year 2000, named model AB2. In this new model some more driving modes are added, namely the Step mode, Gate mode, and DC mode. This study then modified the system by direct digital control with the LabVIEW development software. The AC mode was used only at long travel condition with moderate speed to the approaching point, around one hundred microns before the target position. The Gate mode was followed with pulse command in time interval at low speed to drive the table to around 200nm distance from the target point. Finally, the DC mode was applied in which the driving voltage enabled the moving table to converge to less than 5nm of the target point. The cooperated feedback

signals from the 20μm-pitch scale were processed by the developed software in LabVIEW, as described in the following section.

3. PRINCIPLES OF WAVEFORM PROCESS

3-1 General waveform errors

Any linear scale has output of two sinusoidal waveforms with 90 degrees shift. The waveforms always have some high frequency noises plus three inherent fundamental errors including: (1) DC drifts (p and q) due to the background light and the circuit's DC drift, (2) amplitude variation due to geometric errors of the moving stage, and (3) out of orthogonality (α) due to the improper setting of two photo detectors. Fig. 5 (left) illustrates the distorted waveforms without noises. The corresponding Lissajous diagram will distort from a pure circle to an elliptical shape, as shown in Fig. 5 (right). In the continuous motion the waveforms carrying those three errors may vary along the displacement, as shown in Fig. 6. It will cause the miss count and subdivision error in either the hardware signal processing circuit or the software processing.
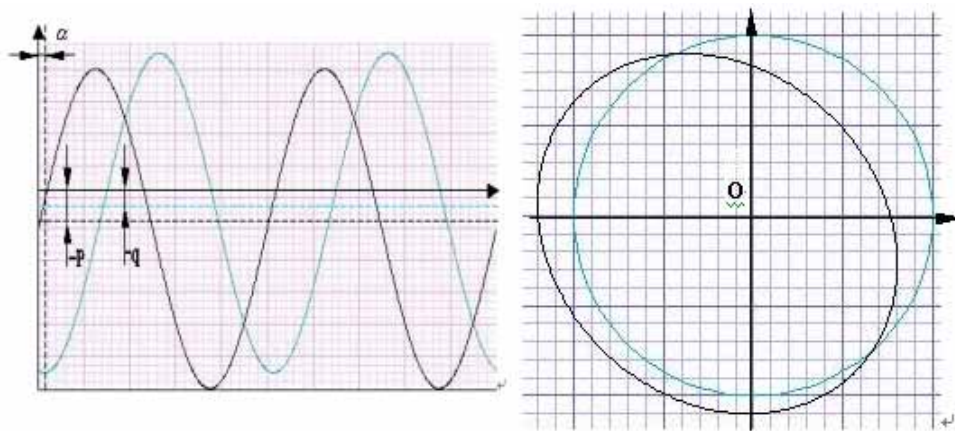

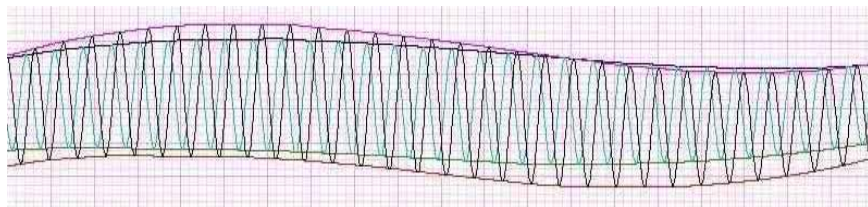Fig. 5: Distorted waveforms and the Lissajous diagram.

Fig. 6: Distorted waveforms in continuous motion

3-2 Long Stroke Displacement by Up/down Counting

The waveform correction scheme should be employed before the signal processing. During the long-stroke motion the DC drift and the amplitude of the output scale waveforms are varied, while α is a constant error dependent only upon the improper separation of two photodiodes. Normal up/down counter with respected to the Schmidt-triggered square waveforms in quarter-pitch is referenced to a given threshold voltage. If the amplitude of the wave falls below the threshold voltage a miss count will occur. Moreover, if the superimposed high frequency noises disturb at the threshold point extra counts will be rendered, as shown in Fig. 7. Solving this problem is the core technology of every counter card company, which treats it as confidential document.
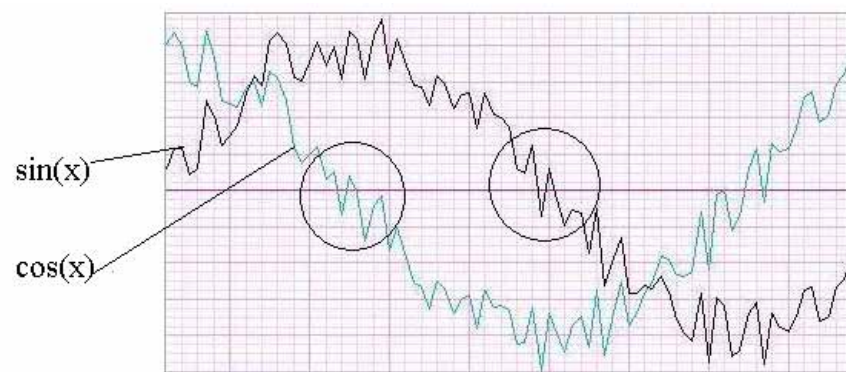

Fig. 7: Noises doped waveforms.

This study applies the software waveform correction strategy developed in LabVIEW. Since α is a constant error dependent only upon the improper separation of two photodiodes, this error can be corrected independently. For the purpose of fast computation only the peaks and valleys of the waveforms are recorded. Four spline curves are fitted to the peaks and valleys of two waveforms respectively, as shown in Fig. 6. All the central points of the two paired curves are adjusted to zero. Taking the average of the amplitudes of the corresponding peak and valley pairs, and normalizing the resulted amplitude to 1, two corrected waveforms of the same amplitude in symmetry to 0 can be obtained, as shown in Fig. 8. Since the information of the phase is not changed, this process will not alter the measured displacement. For the correction of α error, two waveforms can be treated as two vectors slightly out of 90 degrees . With a simple vector summation and subtraction operations, two output vectors can be automatically square to each.
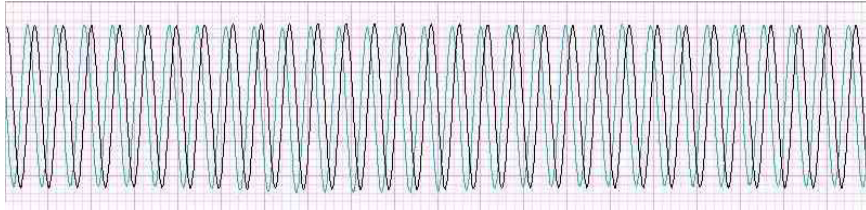
Fig. 8: Corrected waveforms.

The pulse counting process can now be employed directly with respect to the corrected waveforms by software without the necessity of square wave transformation. Assuming the noises are not existed in the corrected sine (say, S1) and cosine (S2) waves, a simple heuristic algorithm can achieve the up/down counting as follows (Fig. 9).

1. If S1 crosses zero from negative to positive while S2 is at negative, count +1, otherwise count -1;
2. If S1 crosses zero from positive to negative while S2 is at positive, count +1, otherwise count -1;
3. If S2 crosses zero from negative to positive while S1 is at positive, count +1, otherwise count -1;
4. If S2 crosses zero from positive to negative while S1 is at negative, count +1, otherwise count -1

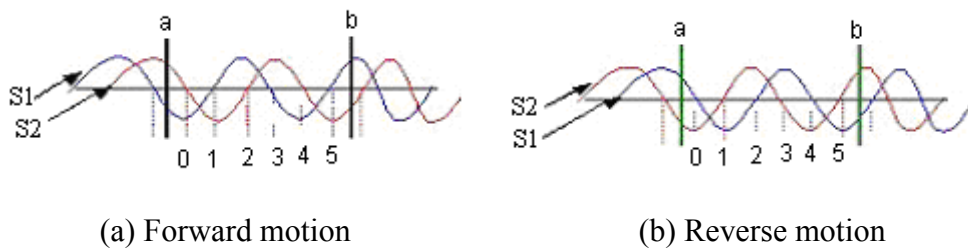(a) Forward motion   (b) Reverse motion

Fig. 9: Pulse counting in forward and reverse motions.

This counting process is simple and straightforward even if the table jitters at the starting and stopping points or the high-frequency noised are added onto the ideal signals. Take an example as depicted in Fig 7, which is frequently happened. When the sin(x) wave moves across zero from positive to negative, the noises will induce three counts with 2-count up and 1-count down. The result is 1-count up, the same as without noises condition. Therefore, this algorithm is robust.

3-3 Methods for Waveform Subdivision

The pulse counting only calculates the displacement to the integral numbers of the quarter pitch. The resolution is still limited to 5μm. For less than quarter pitch motion it has to be done by the subdivision method. With regard to the fringe subdivision technique, although there have been many methods proposed by various researches, such as the curve fitting [4], signal modulation [5] and with CCD [8], there are still either time consuming in software or sophisticate in hardware. This research developed a simple and quick method of the subdivision by fitting an ideal circle to the Lissajous diagram.

As shown in Fig. 9, in the beginning (a) and the final (b) points of the stage motion, incomplete counts are always existed. Taking five cycles, for example, into account, since the travel is short the DC drift and the amplitude variation are only slight. It is reasonable to assume that only the noises superimposed onto the ideal waveforms is of a major effect, as shown in Fig. 10. In order to remove these noises and adjust the slight DC drift and amplitude variation, the strategy of Lissajous circle curve fitting can be applied. Let an ideal equation of the circle be:

$$x = R\sin\theta + a \tag{1}$$
$$y = R\cos\theta + b \tag{2}$$
$$R = \sqrt{(x-a)^2 + (y-b)^2} \tag{3}$$

The values of a and b in Eqs. (1) and (2) indicate the mean DC drifts of two waveforms. The radius R denotes the mean amplitude of the noises removed circle. In the Lissajous diagram recorded amplitudes of two sinusoidal curves are x_i and y_i. Normal curve fitting process with respect to a circle should employ the least-squares error function as

$$F(a,b,R) = \sum_{i=1}^{n}\left[\sqrt{(x_i - a)^2 + (y_i - b)^2} - R\right]^2 \tag{4}$$

where, the objective function F containing three variables has to be minimized. However, in general, no closed form solution exists. It is, therefore, easier to use the so-called algebraic distance [9].

$$G(a,b,R) = \sum_{i=1}^{n} \left[(x_i - a)^2 + (y_i - b)^2 - R^2 \right]^2 \qquad (5)$$

Let G be zero, Eq. (5) can be rearranged to:

$$\sum_{i=1}^{n} (2ax_i + 2by_i + R^2 - a^2 - b^2) = \sum_{i=1}^{n} (x_i^2 + y_i^2)$$

A least-squares solution can be obtained by solving the simultaneous equations of

$$\begin{bmatrix} x_1, y_1, 1 \\ x_2, y_2, 1 \\ \cdots \cdots \\ x_n, y_n, 1 \end{bmatrix} \cdot \begin{bmatrix} 2a \\ 2b \\ R^2 - a^2 - b^2 \end{bmatrix} = \begin{bmatrix} x_1^2 + y_1^2 \\ x_2^2 + y_2^2 \\ \cdots \cdots \\ x_n^2 + y_n^2 \end{bmatrix} \qquad (6)$$

Variables (a, b, R) can be solved with the mathematic tool of LabVIEW. The instantaneous phase (θ) of the beginning point or the end point (A) of the stage can then be easily computed by the arctangent function on the smoothed circle, as shown in Fig. 11.
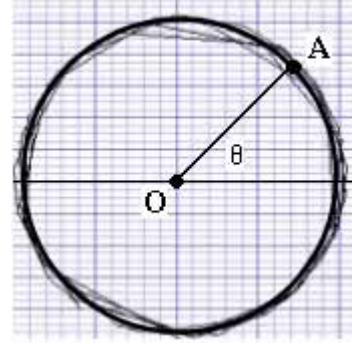

Fig. 10: Fractional wave with continued 5 waves.   Fig. 11: Lissajous circle fitting.

4. POSITIONING CONTROL STRATEGY

To any target position the PCLM stage was commanded to move in three modes. Firstly, in the AC mode, an appropriate voltage was given from the PC to the AB2 driver, through a NI-6711 D/A card, to drive the HR-4 motor. The motion stopped at a predetermined position around 100μm before the target.   Waveforms output from the linear scale were digitized by a NI-6023 A/D card before entering into the LabVIEW software. If the velocity was reducing due to the friction effect of the linear guide a PI control was applied to increase the output voltage. The displacement was detected by

the pulse counts, which were compared with the ideal number of counts with respect to the ideal distance. Instantaneously, during each "while loop" of the sampling process, the pulse count was carried out and in such a short time the DC and amplitude could be seen stable. During the motion pulse count of each "while loop" was added to the total count. The software determines whether the motion should be stopped based on the gross count, though it might not be exactly right. After the AC motion was over, all the signal data could be processed and the waveform correction was carried out. The exact pulse count was obtained.

Secondly, the control loop was switched to the Gate mode, in which a low voltage was given to the AB2 driver in a short interval so that the stage could move with each step less than 200nm. The waveform digitization was continued from the AC mode. The incomplete cycles at the beginning of AC mode and the end of Gate mode were calculated by the Lissajous circle fitting, as described in Sec. 3-3. The exact displacement up to the end of the Gate mode could be computed by total pulse counting and signal subdivision. The position now was close to the target with less than 200nm.

Lastly, switching to the DC mode control, the displacement was proportional to the supplied voltage. Since the step was too small, the instantaneous phase change is not sensitive in the Lissajous diagram. The characteristic curves of DC mode had to be calibrated using a laser interferometer in advance. Fig. 12 shows the schematic diagram of DC motion calibration. This diagram is also applicable to the overall positioning accuracy calibration that will be described in the next section. Because it is a simple piezo actuator motion, the hysteresis effect will appear. The calibration procedure has to be made with the forward and reverse motions individually. Fig. 13(a) shows the DC forward motion calibration results, and the reverse motion results are shown in Fig. 13(b). After the spline curve fitting to each motion the residual errors could be reduced to within 10nm. The repeatability was also controlled to within 10nm. These fitted curves can be used for the feed-forward control of the DC mode motion.
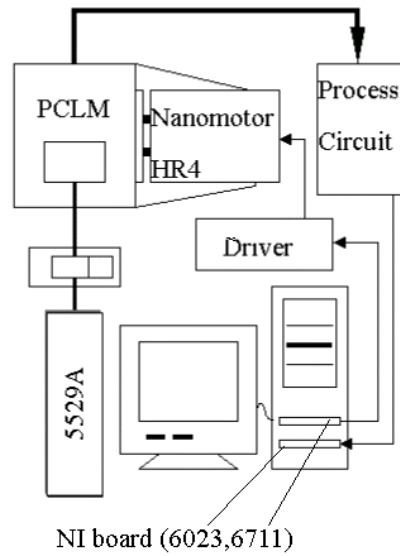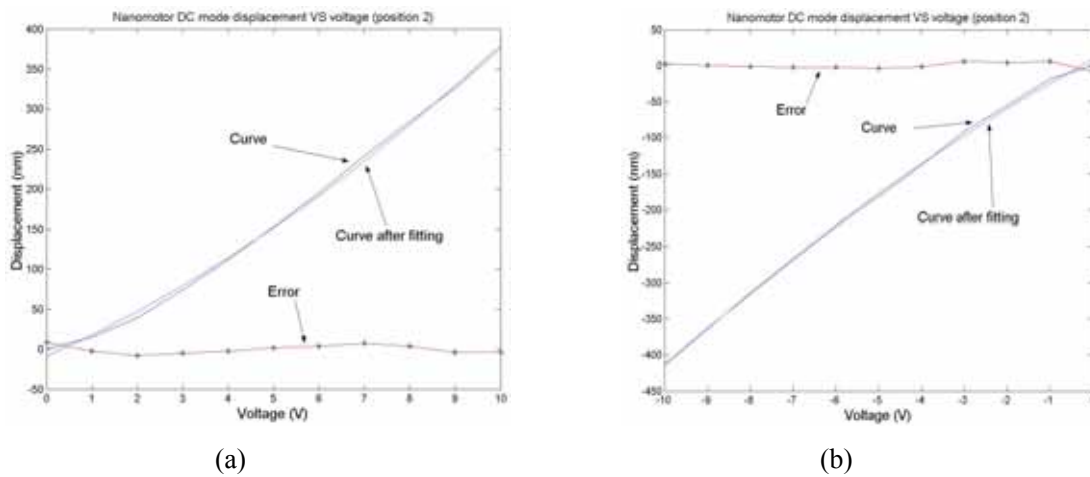
Fig. 12: Schematic diagram of system calibration

(a)   (b)

Fig. 13: Accuracy calibration of DC motion: (a) forward, (b) reverse.

5. VELOCITY CONTROL IN AC MODE

Signals with distortion can be processed by software as indicated in Section 3, but the process itself might introduce new errors. So signals are better with less distortion as possible. Besides, because there are some complicated calculation in each "while loop", which cannot process too many sampled data. Thus, in the AC mode, low and stable velocity is necessary. Classical PID control needs constant parameters K_p, K_i and K_d, which should be determined by experiments. However, if the stage is moving with a non-constant friction condition, the parameters should be dynamically adjusted. In this study a PID control scheme associated with neural network is proposed so that

K_p, K_i and K_d could be adjusted on-line according to the applied control scheme and the self-learning of neural network.

5-1 Velocity Control Diagram

In this study K_p, K_i and K_d are determined and adjusted by BP neural network, which is a multi-input and multi-output system. The velocity control diagram of the integrated BPNN and PID is shown in Fig.14. The structure of neural network is given in Fig.15. The outputs of the neural network are:

$$x_1^{(3)}(k) = K_p$$
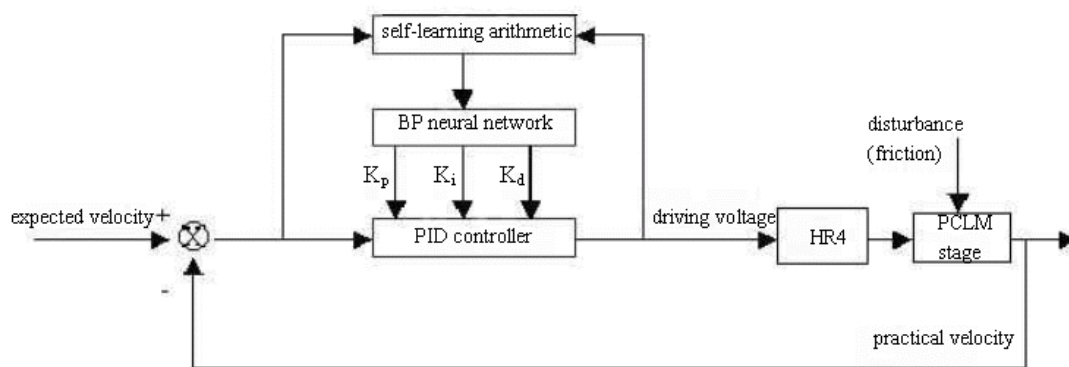
$$x_2^{(3)}(k) = K_i$$

$$x_3^{(3)}(k) = K_d$$

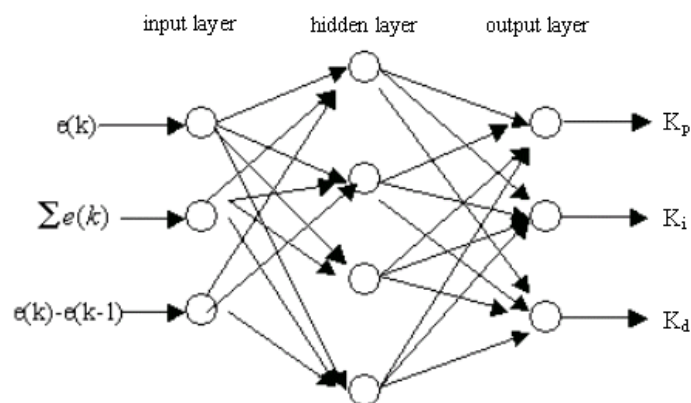Fig.14. The velocity control loop diagram.

Fig.15.The structure of BP neural network.

5-2 Theory of BPNN with PID Control

Classical PID control algorithm can be described as:

$$u(k) = u(k-1) + K_p \left[e(k) - e(k-1) \right] + K_i e(k) + K_d \left[e(k) - 2e(k-1) + e(k-2) \right] \quad (7)$$

where, error e(k) = r(k) - y(k) is the difference of the command value and the output value in every instant. In this study, u(k) is the driving voltage, r(k) is the command velocity and y(k) is the actual velocity.

The BP neural network PID controller in this paper is a supervised learning control. Let the performance index function be the deviation between the command velocity and the actual velocity:

$$J = \frac{1}{2} \left[r(k+1) - y(k+1) \right]^2 \quad (8)$$

Note that J is not constant during the stage motion. The connection weight coefficients in the hidden layer ($\omega_{ij}^{(2)}(k)$) and output layer ($\omega_{li}^{(3)}(k)$) are to be dynamically adjusted in the negative gradient direction of J based on the steepest descent method. In the output layer we define

$$\Delta \omega_{li}^{(3)}(k+1) = -\eta \frac{\partial J}{\partial \omega_{li}^{(3)}} + \alpha \Delta \omega_{li}^{(3)}(k) \quad (9)$$

where, η is the learning rate and α is momentum factor. Inputs and outputs of the output layer are:

$$\begin{cases} net_l^{(3)}(k) = \sum_{i=1}^{Q} \omega_{li}^{(3)} x_j^{(2)}(k) - \theta_l^{(3)} \\ x_l^{(3)}(k) = g \left[net_l^{(3)}(k) \right] \end{cases} \quad (10)$$

where, Q is the neuron number of the hidden layer, $\theta_l^{(l)}$ is the corresponding threshold value, g(x) is activation function in output layer. The differential term in Eq. (9) can be expressed by

$$\frac{\partial J}{\partial \omega_{li}^{(3)}} = \frac{\partial J}{\partial y(k+1)} \cdot \frac{\partial y(k+1)}{\partial u(k)} \cdot \frac{\partial u(k)}{\partial x_l^{(3)}(k)} \cdot \frac{\partial x_l^{(3)}(k)}{\partial net_l^{(3)}(k)} \cdot \frac{\partial net_l^{(3)}(k)}{\partial \omega_{li}^{(3)}}$$

$$\frac{\partial J}{\partial \omega_{li}^{(3)}} = e(k+1) \cdot \frac{\partial y(k+1)}{\partial u(k)} \cdot \frac{\partial u(k)}{\partial x_l^{(3)}(k)} \cdot g'\left(net_l^{(3)}(k) \right) \cdot x^{(3)}(k) \quad (11)$$

From Eq. (7) we have

$$\begin{cases} \dfrac{\partial u(k)}{\partial x_1^{(3)}(k)} = e(k) - e(k-1) \\[2mm] \dfrac{\partial u(k)}{\partial x_2^{(3)}(k)} = e(k) \\[2mm] \dfrac{\partial u(k)}{\partial x_3^{(3)}(k)} = e(k) - 2e(k-1) + e(k-2) \end{cases} \quad (12)$$

So we can get:

$$\begin{cases} \Delta\omega_{li}^{(3)}(k+1) = \eta\delta_l^{(3)}x_i^{(2)}(k) + \alpha\Delta\omega_{li}^{(3)}(k) \\[2mm] \delta_l^{(3)} = e(k+1)\cdot\mathrm{sgn}\left(\dfrac{\partial y(k+1)}{\partial u(k)}\right)\cdot\dfrac{\partial u(k)}{\partial x_l^{(3)}(k)}\cdot g'\left(net_l^{(3)}(k)\right) \end{cases} \quad (13)$$

The connection weight coefficient in the output layer can then be dynamically adjusted by

$$\omega_{li}^{(3)}(k+1) = \omega_{li}^{(3)}(k) + \Delta\omega_{li}^{(3)}(k+1) \quad (14)$$

Similarly, in the hidden layer we can also obtain the real time connection weight coefficient as

$$\omega_{ij}^{(2)}(k+1) = \omega_{ij}^{(2)}(k) + \Delta\omega_{ij}^{(2)}(k+1) \quad (15)$$

Experiments show that when the velocity of the table is controlled to 2mm/s the signals perform the best index function. Fig.16 shows the velocity when it is controlled to 2mm/s by the BPNN and PID control strategy. It is very stable throughout the travel.
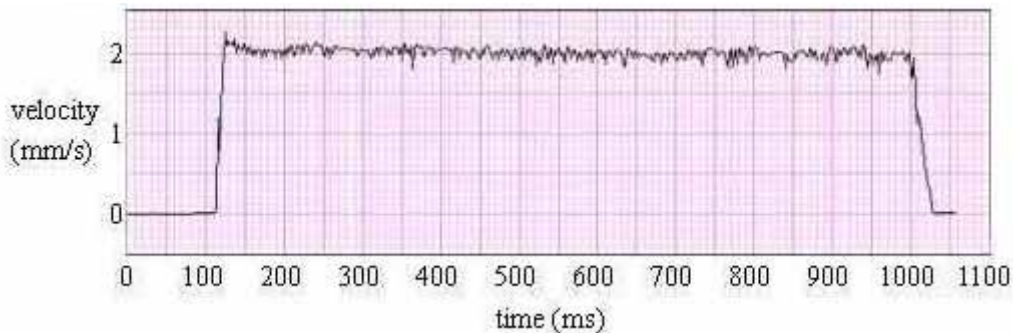

Fig.16. Stage velocity at command 2mm/s with BPNN and PID control.

6. EXPERIMENTAL TESTS

This digital control scheme with software error compensation was testified by positioning experiments of 5 different displacements: 1mm, 3mm, 5mm, 7mm, and 9mm. Each experiment was repeated by five times. The PC gave the positioning commands and the actual displacement was read by the HP5529A laser interferometer,

as shown in Fig. 12. Table 1 lists the first experimental result. It is clearly seen that the positioning errors increase with the stroke lengths. The repeatability is, however, within $\pm 25\,$nm. This is because the optical axis of HP5529A may not be perfectly aligned with the motion axis of the stage. In addition, the grating pitches could also have cumulative errors.

Table 1: Initial positioning tests results.

position⟍time	1mm	3mm	5mm	7mm	9mm
1	1.000188	3.000650	5.001278	7.001589	9.001968
2	1.000159	3.000615	5.001238	7.001569	9.002008
3	1.000139	3.000654	5.001238	7.001548	9.001978
4	1.000168	3.000620	5.001276	7.001552	9.002006
5	1.000139	3.000625	5.001237	7.001585	9.001977
average	1.000159	3.000633	5.001253	7.001569	9.001987
Average error (nm)	159	633	1253	1569	1987
standard deviation (nm)	21	18	22	19	18

A compensation strategy was then applied to correct the systematic errors. In the second test, the commanded positions were corrected to: 0.999841mm, 2.999367mm, 4.998747mm, 6.998431mm, and 8.998013mm respectively. Tested results are shown in Table 2. The positional accuracy has been significantly improved to within 30nm. The standard deviations are slightly increased. It could be due to the worse environmental stability as the time lasted.

Table 2: Compensated positional accuracy

Position⟍time	1 mm	3 mm	5 mm	7 mm	9 mm
1	1.000010	3.000050	5.000069	7.000009	9.000068
2	1.000020	3.000039	5.000012	6.999959	9.000019
3	0.999989	2.999989	5.000002	6.999981	9.000031
4	1.000040	2.999991	5.000030	6,999972	9.000011
5	1.000039	2.999991	5.000042	6.999931	9.000010

average	1.000020	3.000012	5.000031	6.999974	9.000028
Mean error (nm)	20	12	31	-26	28
standard deviation (nm)	21	30	26	29	24

6. CONCLUSIONS

This article presents the developed positioning control strategy on a commercially available PCLM stage. With proposed three motion modes at high, low, and fine velocities, and the corresponding signal processing techniques, this method is able to achieve the nanopositioning control with the precision one order better than the originally listed specifications. In order to obtain high accuracy and fast software computation, some special features are as follows:

1. The LabVIEW 6.0 development tool is used as the system controller.

2. In the AC mode, only the pulse counting process is used. The stage motion is controlled by the integrated BPNN and PID control strategy to assure the constant velocity throughout the travel.

3. In the Gate mode, the pulse counting and Lissajous circle subdivision are implemented.

4. In the DC mode, the feed-forward error compensation scheme is adopted.

For the AC velocity with 5mm/sec, for example, only 5KHz sampling rate is needed for digitizing 20 points per waveform cycle. The LabVIEW software and the NI interface cards are capable to achieve this speed. The residual errors could be due to the uneven grating pitches, the random errors of the PCLM stage, and the temperature variation that causes the instability of the laser interferometer readings.

REFERENCE

[1] Jäger G., Grǔnwald R, Manske E, Hausote T and FuBl R, "A Nanopositioning and Nanomeasuring Machine, Operation Measured Results," Nanotechnology and Precision Engineering Vol. 2, No. 2, 2004, p. 81-84.

[2] Vorndran, S., "Nanopositioning: Fighting the Myths," Opto & Laser Europe,

November 2004.

[3] "Technical Specifications of PCLM Positioning Stage," Anorad Co., USA, 1998.

[4] Brich, K. P., "Optical Fringe Subdivision with Nanometric Accuracy" Precision Engineering, Vol. 12 No. 4, 1990, 195-198.

[5] Chen, B. Y. and Li, D. C., "Progress in Studies on Long-Range and Ultrahigh-Accuracy Nanometer Measurements," Proceedings of the 2nd ISIST, Vol. 2, Jinan, China, 2002, pp. 84-89.

[6] Cui, J., Li, H.Q. and Chen, Q., "New Digital Subdividing and Raster-sensing Technique for Moire Fringe and Grating," Optical Technique, Vol. 26, No. 4, 2000, pp. 294-296.

[7] Chu, C.L., Fan, K.C., and Chen, Y.J., "Design of a Digital Controller for Long-stroke Submicron Positioning stage", Proceedings of the 1st International Conference of Positioning Technology, Act-city, Hamamatsu, Japan, June 9-11, 2004, pp. 176-181.

[8] Wen, P. and Hsu, D. H., "Direct subdivision of Moire fringe with CCD," Proceedings of SPIE, Vol. 1230, 1990, pp. 165-166.

[9] Pratt, V., "Direct Least-square Fitting of algebraic surfaces", Computer Graphics, Vol. 21, No. 4, July 1987, pp. 145-152.

[10] Tao, Y.H., Yin, Y.X., and Ge, L.S., "New PID control and its applications," China Machine Press, Beijing, 1998.